16th World Congress in Computational Mechanics (WCCM)
21-26 July 2024, Vancouver, Canada
A. Korobenko, M. Laforet, S. Prudhomme, R. Vaziri (Eds)

Numerical Simulation Investigation on Nonlinear Flow characteristics of Rough Single Fractures with Different Contact Areas

Yanbo Liang[1], Yuanfang Cheng[2], Zhongying Han[3], Chuanliang Yan[4]

[1]School of petroleum engineering, China university of petroleum(East China),
No. 66, West Changjiang Road, Huangdao, Qingdao,Shandong, China, 266580
E-mail: 1033616923@qq.com

[2]School of petroleum engineering, China university of petroleum(East China),
No. 66, West Changjiang Road, Huangdao, Qingdao,Shandong, China, 266580
E-mail: yfcheng@126.com

[3]School of petroleum engineering, China university of petroleum(East China),
No. 66, West Changjiang Road, Huangdao, Qingdao,Shandong, China, 266580
E-mail: hzy_0218@163.com

[4]School of petroleum engineering, China university of petroleum(East China),
No. 66, West Changjiang Road, Huangdao, Qingdao,Shandong, China, 266580
E-mail: yanchuanliang@163.com

Key words: Rough Fractures, Contact Area, Nonlinear flow, Numerical simulation.

Abstract. To comprehensively understand the influence of the contact area on the flow characteristics of rough single fractures, a rough fracture surface is initially constructed using a spatial frequency domain approach. Subsequently, rough single fractures with varying contact ratios are derived by translating and displacing the fracture surface. The Navier-Stokes equation and Mass-conservation equation are solved by utilizing the laminar flow module integrated within the COMSOL software. The simulation results show that the nonlinear correlation between fluid flow velocity and pressure gradient can be described by using Forchheimer equation. Under the same flow velocity, a higher contact rate will exacerbate the nonlinear characteristics of fluid flow. In contrast to non-contact fractures, the streamlines within contact fractures exhibit increased tortuosity, accompanied by an elongation of flow pathways. Furthermore, with an expanding contact area, the complexity of the streamline pattern amplifies. The overall pressure field distinctly exhibits non-uniform characteristics, with larger pressure gradient observed within localized contact regions, consequently facilitating an increase in flow velocity.

1 INTRODUCTION

Impacted by tectonic movements and human construction activities, numerous fracture networks often develop in underground rock formation. These fracture networks not only control the mechanical properties of the rock mass but also serve as the primary pathways for fluid flow [1-2]. The permeability characteristics of fractured formations are crucial for various

underground engineering constructions, such as unconventional oil and gas extraction [3-5], underground carbon storage [6], nuclear waste disposal [7], mining water inrush, etc. [8]. Understanding the fluid flow behavior of single fracture is essential for studying the permeability characteristics of fractured rock mass.

The Cubic Law based on the parallel smooth plate model has the characteristics of simplicity and efficiency in describing the characteristics of single fracture seepage, and has been widely applied in many engineering constructions. This law assumes that the flow rate through the fracture is proportional to the cubic power of the fracture aperture [9-10]. However, the surface of rock fractures in the natural state is rough and uneven, and the fluid flow calculation results of the Cubic Law are overestimated. Numerous scholars have proposed various modified forms of Cubic Law through indoor tests, mainly taking into account the effects of surface roughness, aperture changing and filling materials on the seepage characteristics of fractures [11-15]. At the same time, some researchers have established local Cubic Laws through theoretical analysis [16-21]. As the flow velocity in the fracture increases, there is a nonlinear relationship between fluid flow rate and pressure gradient due to the dual effects of inertia effect and fracture surface morphology. The Cubic Law and its modified form are no longer applicable. In order to consider the influence of inertia effect, the quadratic term of flow rate is added to supplement the Cubic Law, resulting in the famous Forchheimer's law [22-25]. However, there is a high contact area in high stress fractured rock masses, and research on the nonlinear seepage law of rough single fractures under different contact rate conditions is still incomplete at present [26-33].

This research aims to obtain the seepage characteristics of rough single fractures under different contact area conditions. A rough fracture surface based on the spatial frequency domain method is established firstly. By translating and displacing the fracture surfaces, rough single fractures with different contact rates are obtained. Subsequently, using the laminar flow module embedded in COMSOL, the Navier-Stokes equations were solved to obtain the seepage characteristics of fractures under different contact ratios.

2 BASIC THEORETICAL EQUATIONS

The fluid flow in rock fracture can be described by using Navier Stokes Equations:

$$\rho\left(\frac{\partial u}{\partial t}+u\cdot\nabla u\right)=-\nabla p+\mu\nabla^2 u+f \tag{1}$$

where, ρ is fluid density, u is fluid velocity vector, t is time, p is pressure, μ is dynamic viscosity coefficient, and f is external force term.

The mass conservation equation can be expressed as follows:

$$\nabla\cdot u=0 \tag{2}$$

The Navier Stokes Equation contains a series of variable order partial differential equations, which are extremely difficult to solve numerically, especially in complex geometric domains. If the effect of inertial force is relatively small compared to viscous force, it can be ignored to obtain the Stokes Equation as follows:

$$\mu\nabla^2 u-\nabla P=0 \tag{3}$$

If the viscous force dominates and the fracture surface is relatively smooth, with no obvious tortuosity in the fracture channel, the Stokes Equation can be further simplified to obtain the Reynolds Equation as follows:

$$\nabla \cdot (e^3 \nabla P) = 0 \tag{4}$$

Where, e is the mechanical apeture of fracture.

When the fracture can be regarded as a smooth parallel plate, the Reynolds Equation can further simplify the classical Cubic Law as follows:

$$Q = \frac{we^3}{12\mu} \nabla P \tag{5}$$

Natural fractures contain complex geometric features and hydraulic conditions, and the application of the Cubic Law is limited to some extent. To better describe the nonlinear relationship between flow velocity and hydraulic gradient, the Cubic Law is supplemented with the square of flow rate. The relationship is called the Forchheimer's law:

$$-\nabla P = AQ + BQ^2 \tag{6}$$

The linear coefficient A and nonlinear coefficient B are respectively represented by the following equations:

$$A = \frac{12\mu}{we^3} \tag{7}$$

$$B = \frac{\alpha\rho}{w^2 e^2} \tag{8}$$

Where, w is fracture width, α is inertia resistance which can be determined in experiment results or empirical equations.

Reynolds number is a dimensionless number used to describe fluid velocity, it can be defined as follows:

$$\mathrm{Re} = \frac{\rho Q}{\mu w} \tag{9}$$

The normalized transmissivity can be used to describe the nonlinear characteristics of fluid flow, which can be expressed as follows:

$$\frac{T_a}{T_0} = \frac{1}{1 + \beta \,\mathrm{Re}} \tag{10}$$

Where, T_a is the apparent transmissivity, which can be expressed by this equation, $-\frac{\mu Q}{w(AQ + BQ^2)}$, T_0 is the apparent transmissivity under linear flow state, which can be used to represent by this equation, $-\frac{\mu}{wA}$, β is a dimensionless coefficient.

3 FRACTURE MODEL SET UP

Compared with indoor experiments and actual measurements, numerical simulation does not require expensive measurement equipment or a large number of sample preparation processes, and can efficiently generate rough surfaces in batches based on given surface feature information. Therefore, this study mainly establishes rough random surfaces based on spatial frequency method. In this method, we want to use the following double sum to represent surface height[34]:

$$f(x,y)=\sum_{m=-M}^{M}\sum_{n=-N}^{N}a(m,n)\cos(2\pi(mx+ny)+\phi(m,n)) \tag{11}$$

Where, x and y are spatial coordinates, $a(m,n)$ are amplitudes, $\phi(m,n)$ is phase angles, m and n are frequencies, with Gaussian maximum cutoff values of M and N.

$$a(m,n)=g(m,n)(m^2+n^2)^{-\frac{\eta}{2}} \tag{12}$$

Where, $g(m,n)$ is a random function with a Gaussian distribution, η is the spectral exponent, represents the rate of higher frequency attenuation, and the phase angle ϕ will be sampled from function u, which has a uniform random distribution between - π/2 and π/2:

$$\phi(m,n)=u(m,n) \tag{13}$$

In addition, this research uses the Joint Roughness Coefficient (*JRC*) to characterize the roughness characteristics of fracture surface, and its expression is as follows:

$$JRC=32.2+32.47\lg Z_2 \tag{14}$$

$$Z_2=\left[\frac{1}{n-1(\Delta x)^2}\sum_{i=1}^{n-1}(z_{i+1}-z_i)^2\right]^{1/2} \tag{15}$$

Where, Z_2 is the square root of the slope.

The contact ratio can be expressed as follows:

$$c=\frac{A_c}{A_f} \tag{16}$$

Where, c is the contact rate, A_c is contact area, and A_f is total area of the fracture surface.

The main parameters involved in the spatial frequency domain method include the spatial frequency cutoff values *M, N*, and the spectral exponent η . Therefore, using the Uniform and Gaussian random distribution functions built-in in COMSOL, as well as the summation operator, *M*=*N*=20, $\eta=1.5$ are selected to generate a rough random surface as shown in Figure 1 (a). After calculation, Z_2=0.3481 and *JRC*=17.32 are obtained. Subsequently, the fracture surface was moved by 0.005m in the vertical direction to obtain the upper surface of the fracture, which formed a non-contact fracture with the lower fracture surface. The upper fracture surface is translated by different distances, and boolean operations in the software are used to delete the contact area that overlapped the upper and lower

surfaces to obtain a single fracture with different contact areas, as shown in Figure 1 (b). Then the model is meshed, and the positions near the contact area are locally refined, as shown in Figures 1 (c)-(d), The specific boundary conditions are shown in Figure (b). The inlet flow velocity is selected as 0.1-1m/s, with each increase of 0.1m/s. The outlet is a constant pressure boundary, which is a standard atmospheric pressure of 101325Pa. The rest of the boundaries are non-slip, and the upper and lower surfaces are impermeable. Subsequently, the NS Equation is solved using the built-in laminar flow module in the software. As shown in Figure 2, a total of 5 contact fractures are established in this research. The distance of the upper fracture surface moving along the positive *x*-axis is 0.6mm, 0.7mm, 0.8mm, 0.9mm, and 1mm, respectively, with corresponding contact ratios of 0.33%, 1.32%, 2.72%, 5.12%, and 6.46%. As the moving distance increased, the contact area gradually increased, and the number of large local pores increased.

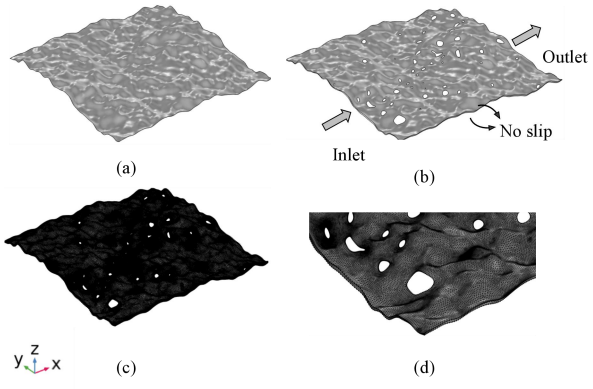

Figure 1: Model set up: (a) single random surface; (b) contact fracture and boundary conditions; (c) mesh division; (d) local mesh refinement.

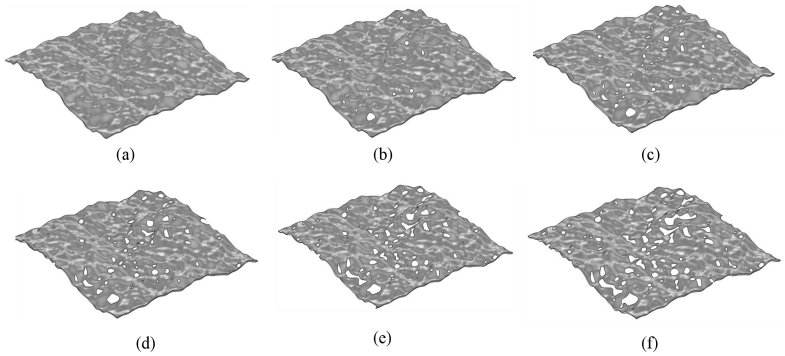

Figure 2: Numerical model of rough fractures with different contact ratios: (a) c=0; (b) c=0.33%; (c) c=1.32%; (d) c=2.72%; (e) c=5.12%; (f) c=6.46%.

The mechanical aperture of fractures with different contact areas is statistically analyzed using built-in functions in the software. The frequency distribution histogram and cloud map are shown in Figure 3. From the frequency distribution histogram, it can be seen that the distribution of the aperture can be described by a Gaussian distribution function. However, the distribution frequency of 0-0.05mm is higher, with frequencies of 0.01, 0.03, 0.05, 0.075 and 0.09, which gradually increase with the increase of contact rate and do not match the Gaussian

distribution. From the cloud map, it can be seen that the aperture in this range is mainly concentrated near the contact area, indicating the presence of many narrow channels near the contact area.

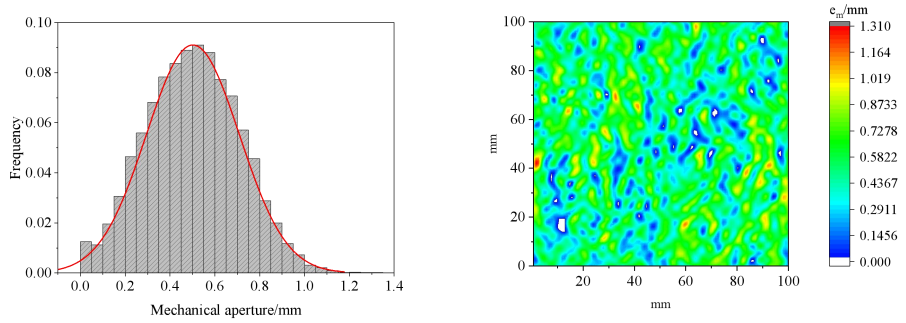

(a)

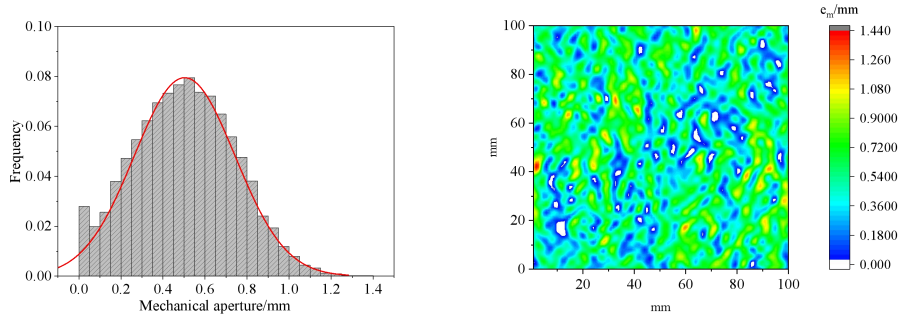

(b)

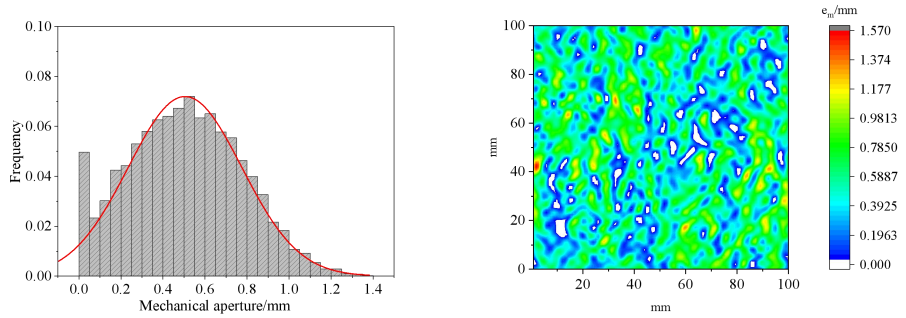

(c)

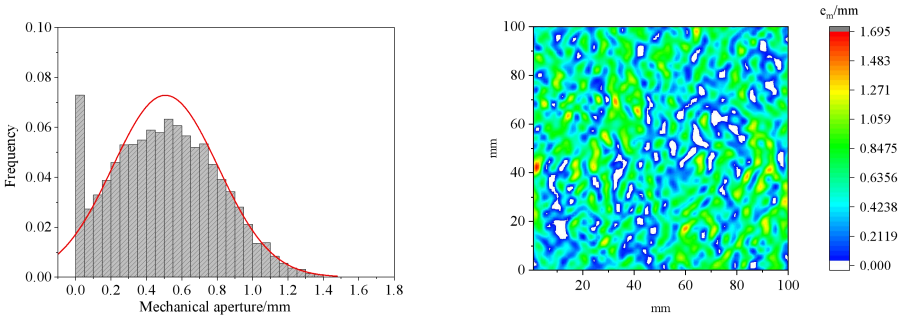

(d)

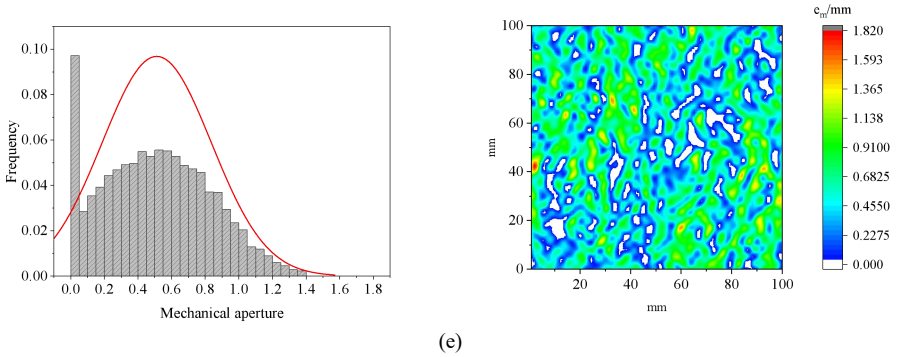

(e)

Figure 3: Mechnical aperture distribution frequency and cloud map undere different contact ratios: (a) c=0.33%; (b) c=1.32%; (c) c=2.72%; (d) c=5.12%; (e) c=6.46%.

4 SIMULATION RESULTS

4.1 Characterization of nonlinear laws

Figure 4 shows the relationship between pressure gradient ∇P and fluid flow velocity Q. The scatter points in this figure represents the simulation results, and the curve is fitted using the Forchheimer equation. It can be seen that the simulation results are highly consistent with the fitted curve, indicating the applicability of the Forchheimer' Law to describe the nonlinear flow of fluid in rough contact fractures. As Q increases, ∇P gradually increases and the rate of increase gradually increases, highlighting the nonlinear flow characteristics. When Q is low, the fluid flow exhibits a certain linear pattern. As the contact ratio increases, the nonlinear effect gradually strengthens. The main reason for this is that when Q is low, the viscous force of fluid motion dominates. As Q increases, the inertia effect of fluid becomes prominent, leading to the gradual enhancement of nonlinear fluid flow. In addition, the presence of contact changes the flow path of fluid, making it more tortuous and exacerbating the nonlinear flow characteristics.

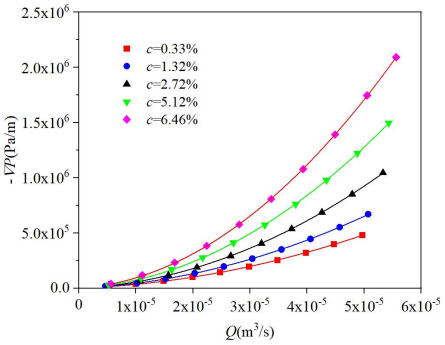

Figure 4: Relationship between pressure gradient ∇P and flow velocity Q.

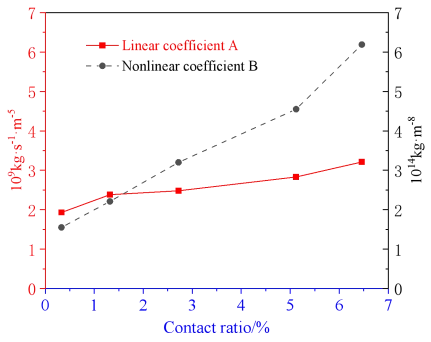

Figure 5: Forchheimer coefficients for fractures with different contact ratios.

The linear coefficient A and the nonlinear coefficient B under different contact ratios are statistically analyzed as shown in Table 1, and a line graph was drawn as shown in Figure 5. The determination coefficients R^2 both exceeded 0.93, further confirming the applicability of

the Forchheimer equation for nonlinear fluid flow in fractures. From Figure 5, it can be seen that the coefficients A and B increase with increasing contact area, and the increase in the linear coefficient A is not significant. The rate of increase in the nonlinear coefficient B is relatively large.

Table 1: Statistics of fitting results of Forchheimer equation

c/%	$A/10^9$kg·s^{-1}·m^{-5}	$B/10^{14}$kg·m^{-8}	R^2
0.33	1.93	1.55	0.93822
1.32	2.38	2.11	0.93854
2.72	2.48	3.2	0.95664
5.12	2.83	4.55	0.93828
6.46	3.21	6.19	0.93857

Table 2: Statistical table of β and Re_c

c/%	β	R^2	Re_c
0.33	0.00837	0.99629	13.27
1.32	0.00932	0.99476	11.92
2.72	0.01373	0.99541	8.09
5.12	0.01731	0.99521	6.41
6.46	0.02018	0.99873	5.50

In general, it is difficult to define the critical flow velocity of fluid to transition from linear flow to nonlinear flow. Therefore, the normalized transmissivity T_a/T_0 can be used to describe the nonlinear characteristics of fluid flow. Figure 6 shows the relationship between T_a/T_0 and Re with different contact ratios. The scatter points in the figure is the result of numerical simulations, and the curve is fitted using Equation (10). From the Figure 7, it can be seen that the overall fitting degree is high. The T_a/T_0 is initially 1, and as Re increases, the T_a/T_0 gradually decreases, and the rate of decrease gradually increases. Under the same flow rate, the contact ratio and T_a/T_0 are inversely proportional, that is, the higher the contact ratio, the smaller the T_a/T_0, and the greater the inertial effect. When T_a/T_0=0.9, it represents that the nonlinear term contributes 10% of the pressure drop. Previous studies have often used the corresponding Reynolds number as the critical flow velocity[35]. The critical Reynolds numbers (Re_c) for single fractures with different contact ratios are 5.50, 6.42, 8.09, 11.92, 13.27, respectively. This indicates that the larger the contact ratio, the smaller the Rec. That is, when the contact area is larger, at relatively small flow velocities, the fluid in the fracture enters a nonlinear flow state.

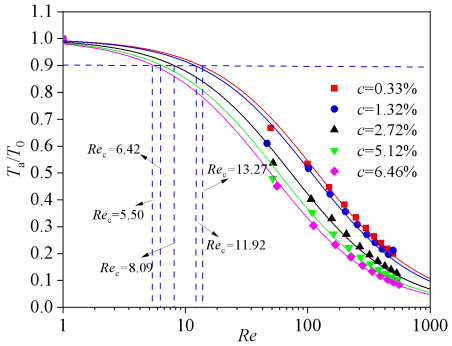

Figure 6: Relationship between Ta/T0 and Re with different c

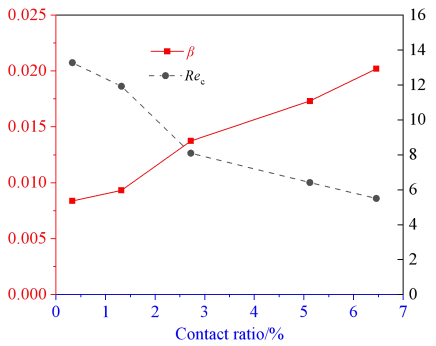

Figure 7: Empirical coefficients β and Rec with different c

4.2 Pressure field distribution

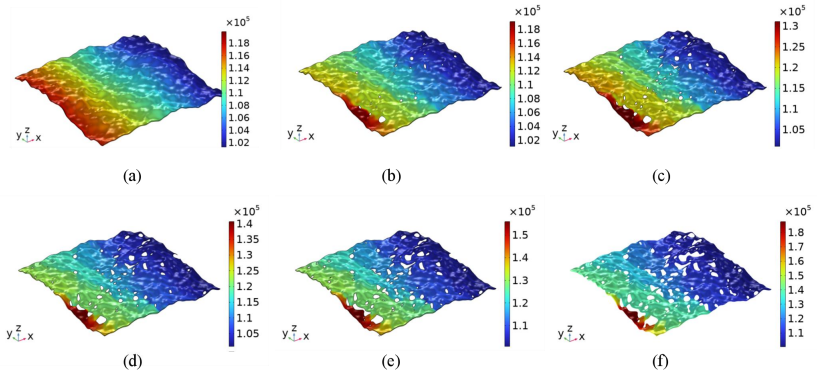

Figure 8: Distribution of pore pressure in fracture with different c (U_{in}=0.5m/s): (a) 0%; (b) 0.33%; (c) 1.32%; (d) 2.72%; (e) 5.12%; (f) 6.64%.

In order to further reveal the influence of contact rate on the nonlinear flow characteristics of fluid in fractures, the distribution law of pore pressure field of rough fractures with different contact areas at an inlet flow rate of 0.5m/s was selected for analysis. As shown in Figure 8, the pressure gradually decreases along the positive x direction. For non-contact fractures, the pressure changes are more uniform and the pressure drop is smaller along the reverse x direction. Compared to non-contact cracks, the presence of contact changes the distribution pattern of pore pressure, and the non-uniformity phenomenon is weak at low contact rates (such as 0.33% and 1.32%) because the fluid has more paths to flow through. As the contact rate increases (such as 2.72%, 5.12%, 6.64%), the non-uniform distribution characteristics of pore pressure become prominent, especially in the vicinity of the contact area, where pressure concentration occurs. The main reason for this is that the presence of contact changes the entire flow space and fluid permeation path of the crack. As the contact rate increases, the available pore space for flow decreases, the flow channel becomes narrower and more complex, and the flow resistance increases, Resulting in an increase in local pore pressure.

4.3 Flow velocity distribution

Figure 9 shows the flow field distribution under different c, with an inlet flow rate of 1m/s. From Figure 9(a), it can be seen that when c=0, although the streamlines fluctuate slightly due to the influence of surface roughness, they are parallel and uniformly distributed as a whole. From Figure 9(b)-(f), it can be seen that compared to the non-contact fracture, the streamline of the contact fractures shows a bending phenomenon, and the degree of bending increases with the increase of contact area. When the c is high, the streamline is significantly twisted and forms complex vortex structures in the local area, indicating that the fluid flow is more disturbed by local geometric structures. The reason for this is analyzed to be the enhancement of fluid inertia effect. In areas of high flow velocity or sudden changes in flow channels, the inertia effect of the fluid becomes significant, leading to the formation of vortices. In terms of flow velocity, when the c is low, the flow velocity is relatively uniform. When the c increases, the local flow velocity undergoes significant changes and becomes very uneven, especially in the narrow part of the fracture, where the flow velocity significantly increases. The main reason for the increase in flow velocity is the increase in contact points,

which leads to an increase in frictional resistance between the fluid and the fracture surface. The fluid must pass through these areas at higher pressure. Secondly, the presence of a large amount of contact narrows the flow channel. According to the principle of mass conservation, the fluid must accelerate in these narrow areas to maintain the same flow rate.

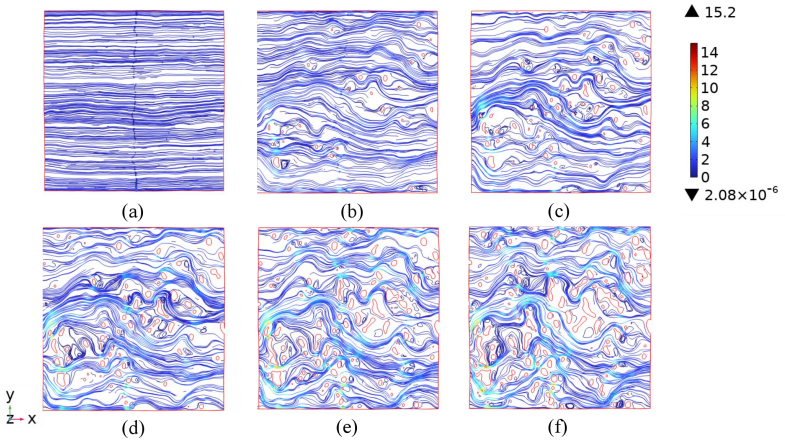

Figure 9: Distribution of streamline and velocity in fractures with different *c* (U_{in}=1m/s): (a) 0%; (b) 0.33%; (c) 1.32%; (d) 2.72%; (e) 5.12%; (f) 6.64%.

5 CONCLUSIONS

Based on the spatial frequency domain method, the rough contact single fractures with different contact ratios are obtained. The NS equation is solved using the built-in laminar flow module in COMSOL to obtain the nonlinear seepage characteristics of fractures under different contact ratios conditions. The specific conclusions are as follows:

1. The nonlinear relationship between fluid flow velocity and pressure gradient can be described by fitting Forchheimer's law. At the same flow rate, a larger contact rate will exacerbate the nonlinear characteristics of fluid flow, and the critical Reynolds number is inversely proportional to the contact rate.
2. As the contact ratio increases, the non-uniform characteristics of the overall pore pressure field become apparent, and the flow channels in the local contact area become complex and narrow, with a large pressure gradient.
3. Compared to non-contact fracture, the streamline of the contact fractures becomes tortuous, the flow path is lengthened, and a complex vortex like streamline structure appears near the contact area. The flow velocity significantly increases in local narrow channels.

REFERENCES

[1] Jiang, Y. J., Li, B. and Tanabashi, Y., Estimating the relation between surface roughness and mechanical properties of rock joints. *Int. J. Rock Mech. Min. Sci.* (2006) **43** (6): 837-846.

[2] Li, X. X., Li, D. Q., Xu, Y. and Feng, X. B. A DFN based 3D numerical approach for modeling coupled groundwater flow and solute transport in fractured rock mass. *Int. J. Heat Mass Transfer.* (2020) **149**: 119179.

[3] Chen, B., Shen, B. T., Zhang, S. C., Li, Y. Y. and Jiang, H., 3D morphology and

formation mechanism of fractures developed by true triaxial stress. *Int. J. Min. Sci. Technol.* 2022 **32** (6): 1273-1284.
[4] Liu, R. C., Jiang, Y. J., Li, B. and Wang, X. S. A fractal model for characterizing fluid flow in fractured rock masses based on randomly distributed rock fracture networks. *Comput. Geotech.* (2015) **65**: 45-55
[5] Liang, Y. B., Cheng, Y. F., Han, Z. Y., Pidho, J. J. and Yan, C. L. Study on Multiscale Fluid–Solid Coupling Theoretical Model and Productivity Analysis of Horizontal Well in Shale Gas Reservoirs. *Energy Fuels* (2023) **37** (7): 5059-5077.
[6] Zhang, Z., Bu, Y., Guo, S., Song, Y., Liu, H., Tian, L. and Lu, Z. Thermodynamic analysis of the corrosion of high alumina cement by carbon dioxide. *J. Clean. Prod.* (2023) **429**: 139417.
[7] Tounsi, H., Rutqvist, J., Hu, M. S., Wolters, R. and Lerche, S. Long-term sinking of nuclear waste canisters in salt formations by low-stress creep at high temperature. *Acta Geotech.* (2023) **18** (7): 3469-3484.
[8] Zhao, J. H., Yin, L. M. and Guo, W. J. Stress-Seepage Coupling of Cataclastic Rock Masses Based on Digital Image Technologies. *Rock Mech. Rock Eng.* (2018) 51 (8): 2355-2372.
[9] Witherspoon, P. A., Wang, J.S.Y., Iwai, K. and Gale, J. E. Validity of Cubic Law for fluid flow in a deformable rock fracture. *Water Resour. Res.* (1980) **16** (6): 1016–1024.
[10] Snow, D. Z. A Parallel Plate Model of Fractured Permeable Media. Univ. of Calif., Berkeley, 1965.
[11] Zimmerman, R. W. and Bodvarsson, G. S. Hydraulic conductivity of rock fractures. *Transp Porous Med* (1996) **23**(1): 1-30.
[12] Neuzil, C. E. and J. V. Tracy J. V. Flow through fractures.*Water Resour.Res*. (1981) **17**(1), 191–199.
[13] Brown, S. R. Fluid flow through rock joints: The effect of surfaceroughness. *J. Geophys. Res.* (1987) **92**(B2), 1337–1347.
[14] Renshaw, C. E. On the relationship between mechanical andhydraulic apertures in rough-walled fractures, *J. Geophys. Res.* (1995) **100** (B12): 24629-24636.
[15] Xiao, W. M., Xia, C. C., Wei, W. and Bian, Y. W. Combined effect of tortuosity and surface roughness on estimation of flow rate through a single rough joint. *J. Geophys. Eng.* (2013) **10** (4): 045015.
[16] He, X. P., Sinan, M., Kwak, H. and Hoteit, H. A corrected Cubic Law for single-phase laminar flow through rough-walled fractures. *Adv. Water Resour.* (2021) **154**: 103984.
[17] Wang, L. C., Cardenas, M. B., Slottke, D. T., Ketcham, R. A. and Sharp, J. M. Modification of the Local Cubic Law of fracture flow for weak inertia, tortuosity, and roughness. *Water Resour. Res.* (2015) **51**(4): 2064-2080.
[18] Ju, Y., Dong, J. B., Gao, F. and Wang, J. G. Evaluation of water permeability of rough fractures based on a self-affine fractal model and optimized segmentation algorithm. *Adv. Water Resour.* (2019) **129**: 99-111.
[19] Qian, J. Z., Chen, Z., Zhan, H. B. and Guan, H. C. Experimental study of the effect of roughness and Reynolds number on fluid flow in rough-walled single fractures: a check of local Cubic Law. *Hydrol. Process.* (2011) **25** (4): 614-622.
[20] Wang, Z. H., Xu, C. S. and Dowd, P. A Modified Cubic Law for single-phase saturated laminar flow in rough rock fractures. *Int. J. Rock Mech. Min. Sci.* (2018) **103**: 107-115.

[21] Hajjar, A., Scholtès, L., Oltéan, C. and Buès, M. A. Effects of the geometry of two-dimensional fractures on their hydraulic aperture and on the validity of the local Cubic Law. *Hydrol. Process.* (2018) **32** (16): 2510-2525.
[22] Forchheimer, P.H. Wasserbewegun durch Boden. *Z. Verein. Dt. Ing.* (1901) **49**: 1736–1749.
[23] Chen, Y. F., Zhou, J. Q., Hu, S. H., Hu, R. and Zhou C. B. Evaluation of Forchheimer equation coefficients for non-Darcy flow in deformable rough-walled fractures. *J. Hydrol.* (2015) **529**: 993-1006.
[24] Li, B., Liu, R. C. and Jiang, Y. J. Influences of hydraulic gradient, surface roughness, intersecting angle, and scale effect on nonlinear flow behavior at single fracture intersections. *J. Hydrol.* (2016) **538**: 440-453.
[25] Rong, G., Yang, J., Cheng, L., Tan, J., Peng, J. and Zhou, C. B. A Forchheimer Equation-Based Flow Model for Fluid Flow Through Rock Fracture During Shear. *Rock Mech. Rock Eng.* (2018) **51** (9): 2777-2790.
[26] Chen, Y., Lian, H., Liang, W., Yang, J., Nguyen, V. P. and Bordas, S. P. A. The influence of fracture geometry variation on non-Darcy flow in fractures under confining stresses. *Int. J. Rock Mech. Min. Sci.* (2019) **113**: 59-71.
[27] Phillips, T., Bultreys, T., Bisdom, K., Kampman, N., Van Offenwert, S., Mascini, A. and Busch, A. A Systematic Investigation Into the Control of Roughness on the Flow Properties of 3D-Printed Fractures. *Water Resour. Res.* (2021) **57** (4): 1-23.
[28] Yin, Q., He, L. X., Jing, H. W. and Zhu, D. Quantitative Estimates of Nonlinear Flow Characteristics of Deformable Rough-Walled Rock Fractures with Various Lithologies. *Processes* (2018) 6 (9): 149.
[29] Javadi, M., Sharifzadeh, M., Shahriar, K. and Mitani, Y. Critical Reynolds number for nonlinear flow through rough-walled fractures: The role of shear processes. *Wat. Resour. Res.* (2014) **50** (2): 1789-1804.
[30] Cunningham, D., Auradou, H., Shojaei-Zadeh, S. and Drazer, G. The Effect of Fracture Roughness on the Onset of Nonlinear Flow. WATER RESOURCES RESEARCH, (2020) **56** (11).
[31] Tzelepis, V., Moutsopoulos, K. N., Papaspyros, J. N. E. and Tsihrintzis, V. A. Experimental investigation of flow behavior in smooth and rough artificial fractures. *J. Hydrol.* (2015) **521**: 108-118.
[32] Xiong, F., Jiang, Q. H., Ye, Z. Y. and Zhang, X. B. Nonlinear flow behavior through rough-walled rock fractures: The effect of contact area. Comput. Geotech. (2018) **102**: 179-195.
[33] Quinn, P. M., Cherry, J. A. and Parker, B. L. Relationship between the critical Reynolds number and aperture for flow through single fractures: Evidence from published laboratory studies. *J. Hydrol.* (2020) **581**: 124384.
[34] Sjodin, B. (2017, June 2). How to Generate Random Surfaces in COMSOL Multiphysics ®. COMSOL Blog. Retrieved from https://cn.comsol.com/blogs/how-to-generate-random-surfaces-in-comsol-multiphysics/(accessed on 2024-02-14).
[35] Yu L, Liu R. C. and Jiang Y. J. A review of critical conditions for the onset of nonlinear fuid fow in rock fractures. *Geofuids*. (2017) **2017**:1–17.